CHEMISTRY OF MATERIALS

Article

pubs.acs.org/cm

Increased Exciton Dipole Moment Translates into Charge-Transfer Excitons in Thiophene-Fluorinated Low-Bandgap Polymers for Organic Photovoltaic Applications

Elisa Collado-Fregoso,[†] Pierre Boufflet,[†] Zhuping Fei,[*,†] Eliot Gann,[‡,§] Shahid Ashraf,[†] Zhe Li,[†,∥] Christopher R. McNeill,[§] James R. Durrant,[*,†,∥] and Martin Heeney[*,†]

[†]Centre for Plastic Electronics, Department of Chemistry, Imperial College London, Exhibition Road, London SW7 2AZ, United Kingdom

[‡]Australian Synchrotron, 800 Blackburn Road, Clayton, Victoria 3169, Australia

[§]Materials Science and Engineering, Monash University, Wellington Road, Clayton, Victoria 3800, Australia

[∥]SPECIFIC IKC, College of Engineering, Swansea University, Central Avenue, Baglan, Port Talbot SA12 7AX, United Kingdom

Supporting Information

ABSTRACT: In this study, we investigate the role of thiophene fluorination in a low-bandgap polymer for organic photovoltaic applications. We use a combined theoretical and experimental approach to investigate charge generation and recombination dynamics, and their correlation with blend microstructure and polymer dipole moment. We find that fluorination results in an increased change in the dipole moment upon exciton formation, which is correlated with the appearance of charge-transfer excitons, as evidenced from ultrafast transient absorption studies. Fluorination also results in smaller yet purer domains, evidenced by atomic force microscopy and resonant soft X-ray scattering, and in agreement with photoluminescence quenching measurements. This change in film morphology is correlated with a modest retardation of nongeminate recombination losses. The efficient charge generation and slower recombination are likely to be partly responsible for the enhanced device efficiency in the fluorinated polymer/fullerene devices.

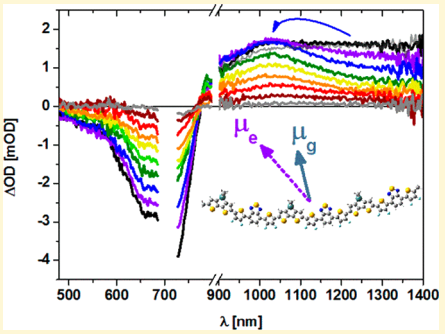

INTRODUCTION

Bulk-heterojunction (BHJ) polymer solar cells have been intensively studied in the past 15 years because of their potential to constitute flexible, lightweight, low-cost devices for energy generation. One of the early strategies adopted to optimize power conversion efficiencies (PCEs) involved the use of low-bandgap polymers which, besides absorbing light in the infrared part of the solar spectrum, can increase the open-circuit voltage of the devices.[1] In this regard, the design of copolymers with different electron densities or donor−acceptor character has been widely used with very positive results.[2−4]

One way to induce a difference in monomer electron density is through the introduction of strong electron-withdrawing atoms such as fluorine,[5] which has resulted in efficiencies as high as 10.8%.[6] Fluorinated polymers often show improved PCEs compared to their nonfluorinated counterparts, although the reasons for this vary according to the system studied.[7−17] In some cases, increasing fluorination leads to detrimental effects on performance, an observation often explained by greater sensitivity to processing conditions due to reduced solubility, and greater tendency of fluorinated polymers to aggregate.[7,11,18,19] Multiple reasons have been suggested to explain the positive effects of fluorination on PCE. The most common of these is the inductively withdrawing nature of fluorine atoms and subsequent stabilization of the highest occupied and the lowest unoccupied molecular orbitals (HOMO and LUMO, respectively). The result is an enhanced open-circuit voltage (V_{OC}), with little or no detrimental effect on the optical band gap, which results in a net gain in efficiency, as long as the energetics still allows efficient charge separation and collection, and the morphology remains similar. However, even replacing a single hydrogen atom on the backbone repeating unit with a fluorine atom rarely leaves the morphology unchanged, and can therefore affect the fill factor (FF) and short-circuit current (J_{SC}). Fluorination tends to considerably enhance aggregation, and as a consequence, blends of fluorinated polymers with fullerene acceptors typically exhibit larger domain sizes, with purer polymer-rich phases than in their nonfluorinated counterparts.[11−14] High domain purity can produce a reduction in both geminate and nongeminate recombination, as observed with time-delayed collection field measurements on a fluorinated version of PCPDTBT (poly[2,6-(4,4-bis(2-ethylhexyl)-4*H*-cyclopenta[2,1-*b*;3,4-*b*′]dithiophene)-*alt*-4,7-(2,1,3-benzothiadiazole)]).[12] This facilitates the collection of charge

Received: July 30, 2015
Revised: October 30, 2015
Published: November 3, 2015

DOI: 10.1021/acs.chemmater.5b02948
Chem. Mater. 2015, 27, 7934−7944

carriers; however, large domain sizes and increased purity can also hamper exciton dissociation by increasing the effective distance the exciton has to travel before reaching the nearest acceptor molecule.[20] Additionally, molecular modeling studies have indicated that partial fluorination of the acceptor unit of the polymer can induce a larger polarization of the polymer excited state, corresponding to an increase in the change in dipole from the ground to the excited state ($\Delta\mu_{ge}$).[13,21−24] Yu and co-workers[25] recently suggested a linear correlation between PCE and $\Delta\mu_{ge}$ as a guideline for material design. The hypothesis behind this relationship is that the increased polarization of excitons generated in polymers with a large $\Delta\mu_{ge}$ facilitates charge separation, by decreasing the exciton binding energy, which ultimately results in an increased J_{SC}. However, this relationship breaks down at higher $\Delta\mu_{ge}$ values, where the acceptor unit is too strong, presumably because of an excessive electron-withdrawing nature of the polymer's acceptor units, which lowers the polymer LUMO level, thus reducing the energetic driving force for charge separation.

Despite the amount of work carried out on polymer backbone fluorination, studies to date have not, to the best of our knowledge, included a detailed spectroscopic analysis of charge separation and recombination as a function of excited-state polarization upon polymer fluorination in polymer/fullerene blend films. With this motivation, we set out to synthesize and investigate two polymers, fluorinated and nonfluorinated, the preliminary results of which were discussed in a previous paper.[26]

While many studies focus on fluorination of the 2,1,3-benzothiadiazole (BT) unit, we opted for the introduction of fluorine atoms on flanking thiophenes (T's), resulting in a TFDTBT (4,7-bis(3,4-difluorothiophene-2-yl)-2,1,3-benzothiadiazole) acceptor unit. Copolymerization of this unit and its nonfluorinated analogue (4,7-bis(thiophene-2-yl)-2,1,3-benzothiadiazole, DTBT) with an alkylated dithieno[3,2-*b*:2′,3′-*d*]germole (Ge) donor unit resulted in directly comparable polymers PGeDTBT and PGeTFDTBT, which for the sake of simplicity will be referred to as F0 and F4, respectively, and are shown in Figure 1. These polymers, previously reported by our group,[26] exhibit similar molecular weights and polydispersities, thus allowing their properties to be fairly compared.

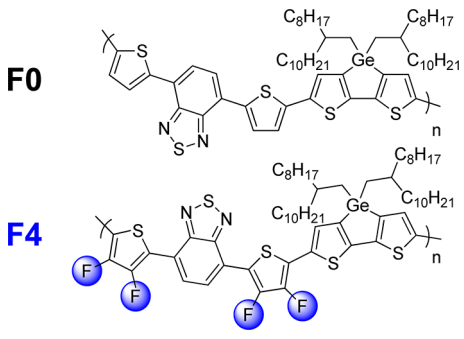

Figure 1. Structures of the polymers studied, PGeDTBT and PGeTFDTBT, referred to here as F0 and F4, respectively.

In our previous study, we demonstrated that fluorination directly results in an increased V_{OC}, related to the lowering of the HOMO level in F4, as well as an almost 2-fold increase in J_{SC} that correlated with a stronger tendency to aggregate as observed by the vibronic features in the F4 UV−vis spectrum, along with the formation of smoother films when mixed with $PC_{70}BM$ ((6,6)-phenyl-C_{70} butyric acid methyl ester), as visible by atomic force microscopy (AFM) (Figure S2).

In this study, we explore the influence of thiophene fluorination on polymer conformation and backbone planarity to explain the changes observed in molecular packing, as well as the effect of fluorination upon the photophysics of neat polymer and polymer/fullerene blend films. Through a combination of time-dependent density functional theory (TD-DFT), grazing-incidence wide-angle X-ray scattering (GIWAXS), resonant soft X-ray scattering (R-SoXS), photoluminescence quenching (PLQ), and transient absorption spectroscopy (TAS), we show that the improvement in device performance upon fluorination is likely to be related to two factors: (1) slower charge recombination from the subnanosecond time scale, which correlates with stronger polymer aggregation and π-stacking in F4 blends as obtained by GIWAXS, and (2) the appearance of polaron-like charge-transfer excitons in the F4 polymer, as observed in ultrafast TAS, which we propose to be related to the equally efficient charge generation observed in F4 blends, despite its lower driving energy for charge generation resulting from a lower lying LUMO level compared to that of F0. This effect is attributed to the strong withdrawing nature of the fluorinated DTBT moiety within the polymer resulting in a high excited-state polarization, as shown by our TD-DFT calculations.

EXPERIMENTAL SECTION

Synthesis. Polymers F0 and F4 were prepared according to the previously reported procedure.[26] Molecular weights and polydispersities (polydispersity index, PDI) were comparable, at 31 kDa (PDI 2.4) and 34 kDa (PDI 2.8), respectively.

Computational Studies. All DFT calculations were performed using Gaussian 09, revision C.01,[27] at either the B3LYP/6-311G(d) or WB97XD/6-311G(d,p) level of theory. Alkyl side chains were replaced by a simple sp^3 methyl group to reduce the computational time. Energies of the DTBT and TFDTBT units as a function of the thiophene−BT dihedral angle were calculated by first optimizing the structure (B3LYP/6-311G(d)) and, using the redundant coordinate editor, running a scan of the dihedral angle in 36 steps of 10° increments. Single-point energy calculations were also performed using WB97XD/6-311G(d,p) for comparison purposes. The resulting energies were converted from hartrees to kilojoules per mole and plotted relative to the respective minima of each structure to give the graph in Figure 2. The minimum energy conformations were then used to calculate the optimized geometries of the donor−acceptor units (WB97XD/6-311G(d,p)). Excited states were calculated using TD-DFT, and correspond to the first excited state, before relaxation.

Film Preparation. All blend films were prepared using the same optimized conditions as for active layers of the best performing devices;[26] that is, they were spin coated from 12 mg/mL 1:2 polymer to $PC_{70}BM$ solutions in *o*-dichlorobenzene (*o*-DCB), after overnight heating at 90 °C. Neat films were spun from a 15 mg/mL polymer solution. All films were kept under a nitrogen atmosphere unless otherwise stated. For GIWAXS measurements, the films were prepared in the same way as for the spectroscopy measurements. For R-SoXS, the films were prepared on sodium poly(styrenesulfonate) (NaPSS)-coated glass slides and subsequently floated off onto silicon nitride membranes.

Steady-State UV−Vis and Photoluminescence (PL) Spectroscopy. Steady-state UV−vis spectra were carried out on all the films used for TAS and PL, with a PerkinElmer Lambda 25 UV−vis spectrometer detecting from 300 to 1100 nm. Steady-state photoluminescence measurements were carried out in neat and blend films of F0 and F4 with a Fluorolog FM-32 spectrofluorometer using either a visible or an infrared detector depending on the fluorescence wavelengths. All the signals were corrected for absorbance at the excitation wavelength. The magnitude of the PL quenching in blend

DOI: 10.1021/acs.chemmater.5b02948
Chem. Mater. 2015, 27, 7934−7944

films was used to estimate the distance L that the exciton diffuses before encountering a fullerene molecule, deconvoluting the polymer and fullerene emission to enable separate determination of their respective PLQ. The following equation was used, as reported previously:[28]

$$L = L_{ex}(1 - \mathrm{PLQ})^{1/2} \quad (1)$$

where L_{ex} is the exciton diffusion length in the absence of quenchers (in the neat film). For the polymer exciton, this was assumed to be 10 nm, a value typical for narrow-band-gap polymers.[29,30] For $PC_{70}BM$, L_{ex} was taken to be 5 nm.[31] We note this analysis neglects the finite size of the exciton, and assumes efficient quenching when a polymer exciton reaches fullerene acceptors. As such, it gives only a relative indication of the length scale of exciton diffusion occurring in the blend films.

Transient Absorption Spectroscopy. Transient absorption spectroscopy on the submicrosecond time scale was performed using a commercial optical parametric oscillator (Oppolette) pumped by a Nd:Yag laser to generate excitation pulses with a time duration of <20 ns and excitation densities of 0.4−30 $\mu J/cm^2$ at 660 nm for the intensity-dependent studies, and 5 $\mu J/cm^2$ for obtaining the transient spectra at 150 ns. Probe light generated from a tungsten lamp was focused onto the sample and then sent to a single grating monochromator. A long-pass filter was placed before the sample to prevent band gap excitation of the sample with the probe light. Transient absorption decays were recorded with the aid of a LabView program referenced to a two-channel oscilloscope, using silicon and InGaAs photodiodes (Costronics Ltd.) for detection in the visible and near-IR, respectively. The time resolution of this setup was 150 ns.

For ultrafast transient absorption spectroscopy, the experiments were carried out with a commercial setup that comprises a 1 kHz Solstice (Newport Corp.) Ti:sapphire regenerative amplifier with 800 nm, 90 fs pulses. The output of this laser was split into two parts that ultimately generate the pump and the probe pulses. The tunable pump pulse was generated in a TOPAS-Prime (Light Conversion Ltd.) optical parametric amplifier and used to excite the sample with energies between 1 and 3 $\mu J/cm^2$ at 710 nm. The probe light was used to generate either a near-IR continuum (900−1450 nm) or a visible continuum (450−800 nm) in a sapphire crystal. A HELIOS transient absorption spectrometer (Ultrafast Systems) was used for collecting transient absorption spectra (450−1450 nm) and decays up to 6 ns. The time resolution of this setup was 200 fs. The samples were kept at all times under a nitrogen atmosphere.

Grazing-Incidence Wide-Angle X-ray Scattering. Measurements were performed at the small-angle X-ray scattering (SAXS)/wide-angle X-ray scattering (WAXS) beamline at the Australian Synchrotron.[32] 11 keV photons were used with 2D scattering patterns recorded on a Pilatus 1M detector. The sample-to-detector distance was calibrated using a silver behenate standard. Scattering patterns were recorded as a function of the X-ray angle of incidence, with the angle of incidence varied from 0.05° below the critical angle of the organic film to 0.2° above the critical angle. The images reported were taken at an angle of 0.3°, well above the critical angle and hence sensitive to the bulk of the film. Data acquisition times of 3 s were used, with three 1 s exposures taken with offset detector positions to cover gaps in the Pilatus detector. X-ray diffraction data are expressed as a function of the scattering vector, $\mathbf{q}$, which has a magnitude of $(4\pi/\lambda)\sin\theta$, where θ is half the scattering angle and λ is the wavelength of the incident radiation.

Resonant Soft X-ray Scattering. Resonant soft X-ray scattering was collected at beamline 11.0.1.2 of the Advanced Light Source at Lawrence Berkeley National Laboratory.[33] Horizontally polarized X-rays at 284.0 eV were aligned normal to the film surface. A 284.0 eV energy was chosen by calculating the scattering materials contrast between the polymers and $PC_{70}BM$. Comparison with nonresonant 270 eV photons determined that the low-$\mathbf{q}$ component of scattering was from roughness, and not materials contrast. Scattered photons were collected by a Princeton PI-MTE in-vacuum charge-coupled device (CCD) detector with 27.6 μm × 27.6 μm pixels. Two scattering patterns of 100 s exposure time were collected at 30 and 150 mm sample to detector distances, respectively, and combined in software. Two-dimensional scattering patterns were reduced to one-dimensional profiles by using a customized version of NIKA.[33]

RESULTS

Device efficiency data for 1:2 F0/$PC_{70}BM$ and F4/$PC_{70}BM$ blends have been reported previously,[26] with F4 blends exhibiting an 80% higher short-circuit photocurrent than F0 blends (7.5 vs 13.5 mA cm^{-2} for F0 and F4 blends, respectively) for blends of similar thickness, as well as an improved open-circuit voltage (0.66 vs 0.71 V for F0 and F4 blends, respectively), resulting in a power conversion efficiency of 5.47% in F4 devices, compared to 3.51% for F0 devices. We note that the F0 and F4 blend films exhibited similar absorption spectra, and absorption coefficients, such that the differences in device performance cannot be assigned to differences in light harvesting, as shown in Figure S1 in the Supporting Information. The increase in V_{OC} was principally attributed to the ca. 0.2 eV reduction in the ionization potential, as measured by both photoelectron spectroscopy in air and cyclic voltammetry.[26] The different FFs for the two devices are suggested to result from changes in the charge collection efficiency for the two cells, as a result of different blend morphologies. We note that the overall efficiency of the devices may be partly limited by the relatively thin blend films (ca. 80 nm) utilized, which may limit light absorption. Attempts to fabricate thicker films in the case of the fluorinated polymer were limited by the solubility of the polymer, which is partly attributed to its high tendency to aggregate.

Theoretical Calculations. *Conformational Analysis.* The conformation of the DTBT unit, fluorinated or not, has been the subject of much debate in recent years.[13,18,34] Indeed, the thiophene can exist with the sulfur atom either on the same or opposite side of the thiadiazole unit of BT. The substitution pattern on the flanking thiophenes has been shown to affect the preferred relative orientation.[13] We investigated the relative conformation of the two monomers DTBT and TFDTBT using DFT calculations, before performing calculations on the full donor−acceptor unit. Initially, the conformation was probed using the B3LYP functional, and a basis set of 6-31G(d), in the interest of saving computational time and to allow ready comparison to many published works which use this functional. The dihedral angle between one thiophene and the BT unit was fixed (see the highlighted bonds in Figure 2), and the rest of the structure was allowed to relax to the minimum energy conformation. These energies were calculated at 10° increments, covering a full rotation of a thiophene ring. The nonfluorinated thiophene appears to prefer having the sulfur atom on the opposite side of the heteroaromatic part of the BT unit (*anti* conformation). In contrast, the fluorinated thiophene in this conformation exhibits an energy maximum. In the latter case the closest local minima are significantly twisted out of plane by about 40°, and are therefore still rather high in energy due to reduced conjugation. Both systems also have an energy minimum with the thiophene moiety pointing in the same direction as the BT unit (*syn* conformation), but while the system is completely planar in the F4 case, it is twisted by about 10° in the F0 analogue, and is therefore slightly higher in energy than the *anti* conformation. Since the B3LYP functional suffers from an overdelocalization error and often inadequately represents dispersive forces, we checked the results by performing similar calculations using the WB97XD functional

DOI: 10.1021/acs.chemmater.5b02948
Chem. Mater. 2015, 27, 7934−7944

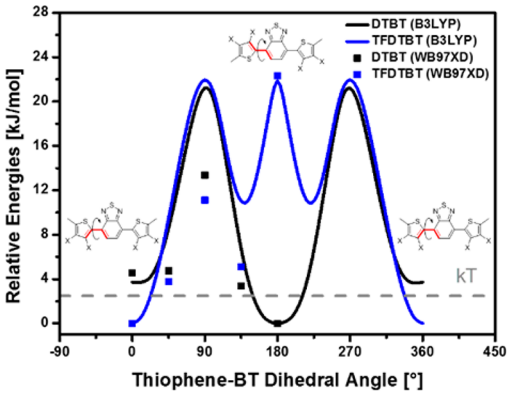

Figure 2. Relative energy of DTBT (black) and TFDTBT (blue) units as a function of the thiophene−BT dihedral angle. X = H or F. Minimum energy conformations are at 180° for DTBT and 0°/360° for TFDTBT. DTBT also exhibits a low energy local minima at 10° and 350°. The dashed gray line represents *kT* at room temperature.

(with a 6-311G(d,p) basis set), which includes a long-range correction and accounts for dispersive forces.[35] To minimize the computational time, selected dihedral angles, from 0° to 180° were calculated. As shown in Figure 2, both functionals support the switch in preferred conformation upon fluorination, as well as the high-energy *anti* conformation for TFDTBT. The barrier to rotation between *syn* and *anti* local minima is, however, significantly overestimated by B3LYP calculations, in agreement with other studies on torsional potentials.[36,37] In both cases though, the barrier is significantly lower for the fluorinated versus the nonfluorinated materials. We note that preference for the *anti*−*anti* (*a*−*a*) for DTBT agrees with the single-crystal structure published for a 4-methylated analogue,[38] whereas lengthening the side chain to hexyl results in a crystal with an *anti*−*syn* (*a*−*s*) conformation.[39]

The crystal structure of the unsubstituted DTBT shows substantial conformational disorder, but with a majority *a*−*s* conformation.[40,41] In all cases, deviations from a fully coplanar backbone are observed (ca. 5−6°). This planarization and apparent switch in conformational preference can potentially be explained through hydrogen-bonding-type interactions (N−H and F−H), or electrostatics.[37,42] The DFT calculations show that while the hydrogen atoms present on the thiophene ring exhibit a partial positive charge (Mulliken), fluorine atoms in the same positions have a partial negative charge of a greater magnitude.

Since the partial charges on the BT unit remain unchanged, the electrostatically favored conformers are reversed upon fluorination (Figure 3). As the DTBT unit contains a plane of symmetry, both thiophenes adopt the same orientation. Therefore, while DTBT prefers the conformation where both thiophene units point *anti* to the BT unit (*a*−*a*), the TFDFTBT unit prefers a *syn* relation for the thiophene and BT units (*s*−*s*). The results of our DFT calculations closely mirror those of previously reported studies for the DTBT unit.[13,18] As Mulliken charges have been shown to inconsistently predict charges for certain heteroatoms, we performed calculations on the *s*−*a* conformer using the CHelpG-based electrostatic potential fit for further confirmation.[37] We indeed observed a slight difference in the magnitude of the charges, but no change in signs of the atoms of interest.

The main conclusion of the calculations is that TFDTBT is likely to show a preference for the planar *s*−*s* conformation. Experimentally, we observed that the F4 polymer has a higher tendency to aggregate in solution than the F0 polymer, and as discussed later, the GIWAXS results also show a smaller π-stacking distance of F4 over F0. Both results would tend to support a more coplanar backbone.

Change in Dipole Moment from Ground- to Excited-State ($\Delta\mu_{ge}$) Calculations. Yu and co-workers first suggested that the magnitude of differences in the ground- and excited-state dipoles ($\Delta\mu_{ge}$) for various donor−acceptor systems correlated with solar cell performance. They suggested that a larger $\Delta\mu_{ge}$ would lower the Coulumbic binding energy of the exciton and facilitate charge separation.[8,21] They calculated ground- and excited-state dipoles for one repeat unit of the donor and acceptor comonomer using the Austin model (AM1), although

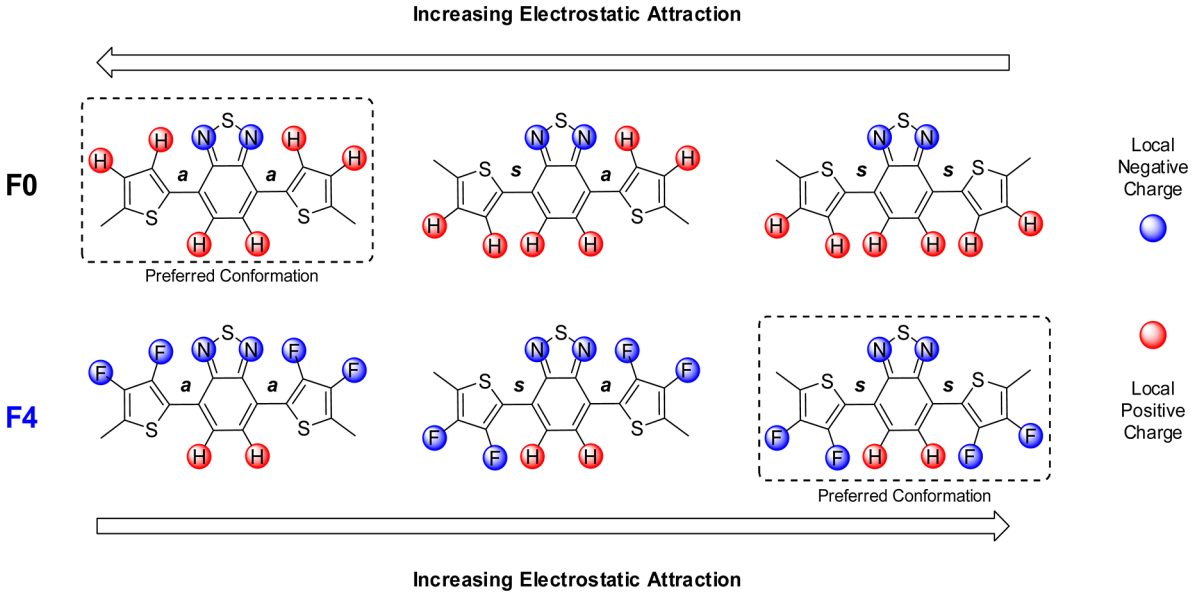

Figure 3. Effect of fluorination on the electrostatics of the DTBT unit, and consequences for the preferred conformation. Reversal of charge from hydrogen to fluorine inverts the preferred conformer from *anti*−*anti* (*a*−*a*) to *syn*−*syn* (*s*−*s*).

DOI: 10.1021/acs.chemmater.5b02948
Chem. Mater. 2015, 27, 7934−7944

others have used DFT (B3LYP).[13] Recently, Ratner highlighted that accounting for all possible minimum energy conformations is crucial to understand and interpret the results from DFT calculations, particularly when considering energy levels and dipole moments.[37] We therefore computed the dipoles in both the ground and excited states for the various possible conformations of each polymer using DFT and TD-DFT, both at the B3LYP level in accordance with previous reports,[13] as well as at the WB97XD/6-311G(d,p) level of theory, which as noted earlier accounts better for dispersive forces. $\Delta\mu_{ge}$ was then calculated by accounting for the *x*, *y*, and *z* components of the dipole moment in the ground and excited states, as outlined by Yu and co-workers.[8] Table 1 shows the data for WB97XD,

Table 1. Ground- and Excited-State Dipole Moments for F0 and F4 Monomer Units with Different Conformations Calculated Using WB97XD/6-311G(d,p)[a]

		a-a	*s-s*	*s-a*	*a-s*
F0	μ_g (D)	2.28	0.29	1.23	3.18
	μ_e (D)	7.07	5.39	5.30	8.03
	$\Delta\mu_{ge}$ (D)	**5.53**	**5.19**	**5.04**	**5.62**
F4	μ_g (D)	5.24	4.60	2.82	3.00
	μ_e (D)	11.41	8.20	8.49	9.12
	$\Delta\mu_{ge}$ (D)	**7.78**	**6.31**	**7.06**	**6.95**

[a]The shaded values are for the lowest energy conformation. In all cases $\Delta\mu_{ge}$ is larger for F4 than for F0.

and the data from B3YLP are shown in the Supporting Information (Table S1). Although the values of $\Delta\mu_{ge}$ are substantially different for the two different functionals (with B3YLP being consistently higher), the trend that fluorination results in a noticeable increase in $\Delta\mu_{ge}$ is consistent for both calculations. We also note that although the conformation of the DTBT and TFDTBT units plays a role in the value of $\Delta\mu_{ge}$, in all cases F4 consistently exhibits a higher $\Delta\mu_{ge}$ than F0 for the equivalent conformation.

When we consider the respective minimum energy conformations (*a*−*a* for F0 and *s*−*s* for F4), $\Delta\mu_{ge}$ increases from 5.53 to 6.31 D upon fluorination (see the values in Table 1). This is mainly due to a greater change in the *x* component of the dipole moment of F4, which lies along the length of the polymer backbone. This effect is predominantly attributed to fluorine atoms increasing the acceptor strength of the TFDTBT unit relative to the DTBT analogue. As a consequence, we can reasonably deduce that excitons produced on the F4 backbone will be more polarized along this axis. In the interest of establishing whether the high $\Delta\mu_{ge}$ for F4 could indeed be related to increased charge generation, picosecond- to microsecond-resolved TAS measurements were performed, the results of which are presented below.

Microstructure and Morphology of Neat and Blend Materials. The morphology of the blend films was investigated by a combination of AFM, R-SoXS, GIWAXS, and PLQ. On relatively large length scales (on the order of 100 nm), F4 and F0 appear to have quite significantly different morphologies. Both AFM and R-SoXS measurements suggest smaller domain sizes for the F4 blend compared with the F0 analogue, with R-SoXS revealing typical domain spacings (long period) of around 90 and 150 nm for F4 and F0, respectively (Figures S2 and S3 in the Supporting Information). The reduced domain size for the F4 blend compared to the F0 blend is different from what has been observed for other copolymers containing the DTBT unit;[12−14] however, the increased aggregation of the F4 polymer compared to the F0 polymer may result in smaller domains.[43,44] Comparing the integrated area of the R-SoXS scattering profiles provides information about the relative purity of these domains,[45] with relative purities of 100% for the F4 blend and 68.6% for the F0 blend. PLQ results (vide infra) show that the emissions of both polymers are nearly entirely quenched upon blending with $PC_{70}BM$, suggesting very fine, nanoscale mixing of the polymers with the fullerene acceptor within the domains revealed by AFM and R-SoXS. The GIWAXS results (Figure S4 in the Supporting Information) show only weak crystalline order in neat films, with alkyl stacking peaks just visible. Both polymers have similar lamellar stacking distances (2.3 nm), with a higher alkyl stacking coherence length for F4 (∼8 nm) compared to F0 (∼5 nm). π-Stacking peaks are also observed, with a significantly lower π-stacking distance of 0.35 nm for F4 compared to 0.40 nm for F0; F4 also has a larger π-stacking coherence length of 4−6 nm compared to <2 nm for F0. Thus, fluorination of the DTBT unit enhances the degree of order in the π-stacking direction, an effect also observed by other groups.[13,46] F4 also tends to adopt a more edge-on orientation than F0. The microstructural properties of F0 and F4 are more or less preserved in blends with $PC_{70}BM$.

The overall morphological picture that emerges from these studies is that fluorination leads to smaller, yet purer, domains, with increased molecular order in the form of π-stacked polymer chains.

Photoluminescence Quenching. To gain more insight into the degree of intermixing of $PC_{70}BM$ and the polymers, photoluminescence measurements in both the neat and the blend materials were performed, probing the quenching of polymer and fullerene PLQ in the blend films. To obtain the polymer PLQ, we excited at 710 nm and detected in the near-IR region. As apparent from Figure 4, emission from both the F0 and F4 polymers in the blends with $PC_{70}BM$ is highly quenched (98% for F0 and 95% for F4 compared to their respective neat materials).

Analysis of this PLQ using eq 1 (and assuming a 10 nm polymer exciton diffusion length) indicates that polymer excitons diffuse only 1−2 nm before being quenched by an acceptor fullerene for both blends. Such short diffusion distances suggest a high level of $PC_{70}BM$ intermixing within the polymer-rich domains, and the absence of a significant fraction of large, pure polymer domains. Although coherence lengths as large as 8 nm in the alkyl stacking direction are observed, the overall degree of crystallinity appears to be low, with the PL quenching data reflecting the majority of polymer chains which are disordered. The slightly lower quenching observed in the F4 blend suggests a modest decrease in the intermixing between the polymer and $PC_{70}BM$, consistent with the R-SoXS results discussed above.

For the fullerene PLQ, we excited the blend films at 475 nm and monitored fullerene singlet exciton emission from 650 to 800 nm. As can be observed in Figure 5, the quenching relative to a neat $PC_{70}BM$ film is noticeably lower as compared to the

DOI: 10.1021/acs.chemmater.5b02948
Chem. Mater. 2015, 27, 7934−7944

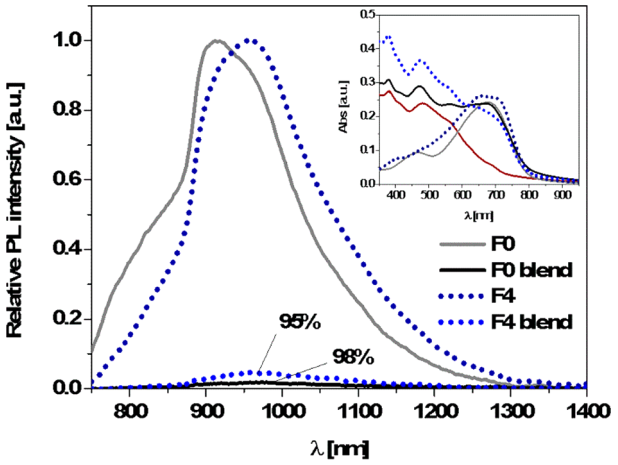

Figure 4. Steady-state photoluminescence (PL) of neat F0 and F4 and their respective blends with $PC_{70}BM$ after excitation at 710 nm, normalized at the respective neat polymer signal maximum. PL quenching was calculated as $PLQ = (1 - PL_{blend}/PL_{neat})$. All signals were corrected for absorbance at 710 nm. The inset shows the UV–vis spectra of the neat and blend films.

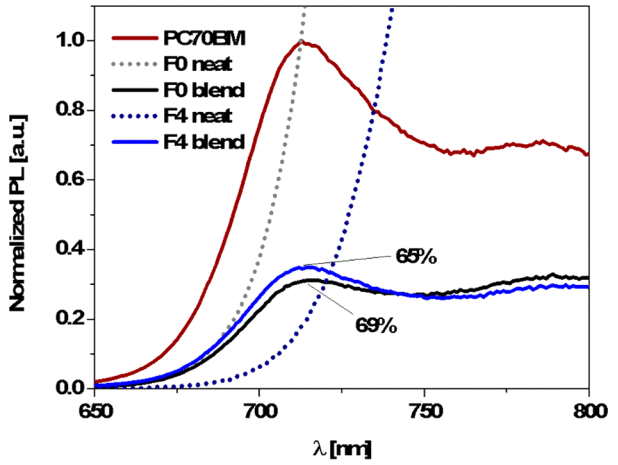

Figure 5. Steady-state photoluminescence (PL) of a neat $PC_{70}BM$ film and F0 and F4 blends after excitation of the fullerene at 475 nm, normalized at the respective neat fullerene signal maximum. All signals were corrected for absorbance at 475 nm.

polymer quenching (69% for the F0 blend and 65% for the F4 blend), suggesting the presence of relatively large, and relatively pure, fullerene domains. Assuming a $PC_{70}BM$ exciton diffusion length of 5 nm, these PLQ data suggest that pure fullerene clusters have a size of ~6 nm. This low fullerene PLQ obtained is indicative of fullerene exciton diffusion being a significant limitation for the efficiency of photocurrent generation for the materials systems studied herein. We note, however, that despite the higher polymer PLQ than the fullerene PLQ, the external quantum efficiency (EQE) in the blue spectral region is still higher than that of the red region.[26] If we assume that the differences in optical interference are negligible for different excitation wavelengths, these results suggest that additional losses, apart from exciton quenching, limit photocurrent generation from polymer excitons, as we discuss in the following sections.

Transient Absorption Spectroscopy. We used femtosecond- to microsecond-resolved TAS as a probe of exciton and polaron dynamics following polymer excitation in both neat polymer films and blends with the $PC_{70}BM$ acceptor. In Figure 6 we show the transient absorption spectra (from 200 fs to 6 ns) of the (a) neat nonfluorinated F0 polymer, (b) 1:2 F0/$PC_{70}BM$ blend, (c) neat fluorinated F4 polymer, and (d) 1:2 F4/$PC_{70}BM$ blend. Films were excited at 710 nm with a beam intensity of 3 $\mu J/cm^2$, and are corrected for differences in absorbance at the excitation wavelength. These conditions ensure, first, that the excitation is selective for the polymer and, second, that nonlinear processes are minimized, since this excitation intensity produces signals within the linear response region (analogous data taken at lower, ~1 $\mu J/cm^2$, excitation densities show similar results; see Figure S5 in the Supporting Information).

We first present the neat spectra for both polymers, and discuss the details of exciton generation and decay (Figure 6a,c). Then we discuss charge generation and recombination from the analysis of the F0 and F4 blend spectra in Figure 6b,d.

One can observe that the spectra for both F0 and F4 neat films show two main types of signals. First, a negative feature from ~550 to 790 nm for F0 and from ~480 to 775 nm for F4 is observed. This negative signal corresponds to polymer ground-state bleaching (GSB), i.e., the depletion of ground-state polymer molecules after excitation, and to stimulated emission (SE). Second, a positive photoinduced absorption band is apparent, extending from ~900 to 1400 nm in both polymers. This photoinduced absorption is assigned to $S_1 \rightarrow S_n$ singlet exciton absorption, consistent with literature assignments of analogous data for other low-bandgap semiconducting polymers.[47−49] From the decay of these positive, photoinduced absorption signals, average decay times for the singlet excitons can be extracted, corresponding to $\tau_{F0} \approx 90$ ps for F0 and $\tau_{F4} \approx 180$ ps for F4. For both polymers, a small, long-lived, residual signal is observed at 6 ns. To determine whether this long-lived signal should be assigned to polaron or triplet states, microsecond-resolved TAS was performed on the neat polymer films in the presence of nitrogen and oxygen atmospheres; see Figure S6a,b in the Supporting Information. In both cases, we found small but detectable signals under both atmospheres, with spectra similar to the residual spectra observed in our ultrafast data at 6 ns. F4 exhibited a larger amplitude and slower decay kinetics compared to F0 ($\tau_{T(F4)} \approx 1.1 \pm 0.07$ μs and $\tau_{T(F0)} \leq 0.7$ μs) when measured in nitrogen. F4's microsecond transient absorption signal is strongly quenched when exposed to an oxygen atmosphere; following literature studies,[50−53] observation of strong oxygen quenching indicates this signal should be assigned to triplet excitons. For the F0 film, the shorter lifetime and smaller signal amplitude prevented us from observing such oxygen-induced quenching, although it appears most likely that this long-lived signal also derives from photogenerated polymer triplet states.

Returning to the description of the ultrafast transient spectra, it is also apparent that the photoinduced absorption of the neat F4 film shows a pronounced, rapid blue shift along with an amplitude increase, such that a band can be observed at 1030 nm from early times. This blue-shifting process exhibits a time constant of ~2.3 ps (see Figure S7 and Table S2). We rule out that the blue shift corresponds to a rapid intersystem crossing, since this would result in an essentially complete quenching of the steady-state PL. We will discuss the importance of this blue shift further below. An analogous, but much weaker blue shift is also observed for F0.

Now we turn to the description of the spectral dynamics of the F0/$PC_{70}BM$ and F4/$PC_{70}BM$ blend films, and discuss

DOI: 10.1021/acs.chemmater.5b02948
Chem. Mater. 2015, 27, 7934−7944

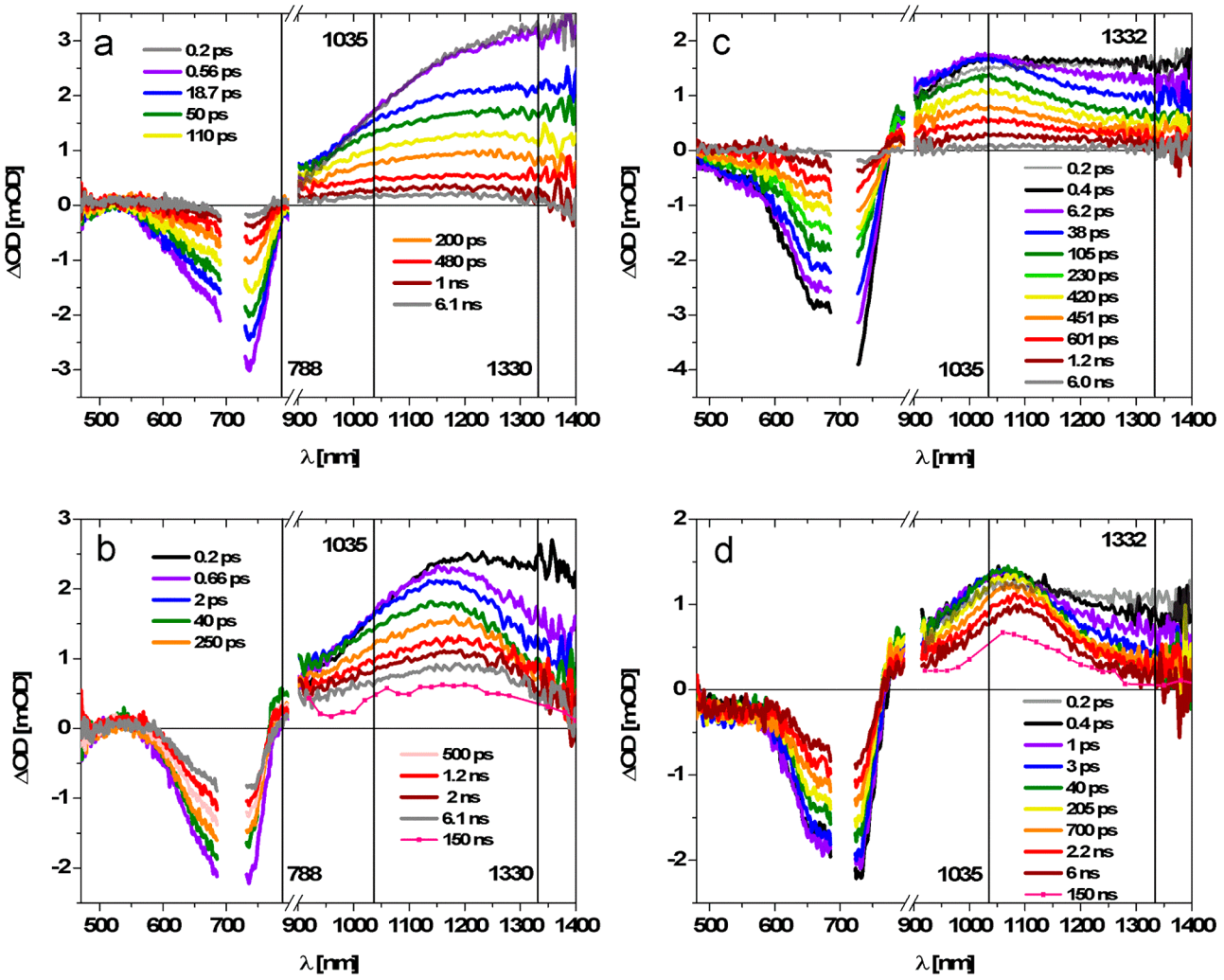

Figure 6. Transient absorption spectra after pump excitation at 710 nm, with a beam intensity of 3 μJ/cm^2 for the (a) F0 neat film, (b) 1:2 F0/$PC_{70}BM$ blend, (c) F4 neat film, and (d) 1:2 F4/$PC_{70}BM$ blend. All signals have been corrected for polymer or blend absorbance, depending on the data belonging to neat polymer or blend transient absorption, respectively. Data with dots were measured in our nanosecond to microsecond setup, 150 ns after excitation at 660 nm, and were corrected to match the beam intensity.

charge generation and recombination after photoexcitation. In Figure 6b,d, absorption features broadly similar to the ones for the neat films can be observed: a negative signal in the visible assigned to GSB and a positive photoinduced absorption signal in the near-infrared (NIR). It is apparent that the GSB signal decay is much slower than that observed for the neat films. At early times, for both blends, the spectrum of the NIR photoinduced absorption is similar to that observed for the neat films, indicative of the initial formation of polymer singlet excitons. This photoinduced exciton absorption, however, is rapidly quenched, with the transient spectra rapidly evolving to a new, blue-shifted absorption signal exhibiting a maximum at ~1150 nm for F0 and ~1100 nm for F4, still present at 6 ns. We notice that the GSB negative signal also has a much larger amplitude at 6 ns compared to the corresponding neat film signal.These observations confirm the presence of long-lived species. We notice the lack of any spectral features corresponding to $PC_{70}BM$ excitons for either blend film, consistent with our excitation wavelength being selective for polymer excitation. To assign the nature of the long-lived blue-shifted signals, we performed submicrosecond TAS on the blend films. As can be observed in Figure 6b,d, the spectra obtained at 150 ns are consistent with the 6 ns spectra. Moreover, the μs-TAS transients (Figures S6c,d and S10 in the Supporting Information) indicate that both blends exhibit oxygen-independent, power law decays that can be assigned to nongeminate recombination of polymer polarons, as previously described in a number of TAS studies in polymer/fullerene systems.[54−58] For F4, this assignment is particularly clear, with the blend film showing no evidence of the oxygen-dependent triplet decay kinetics observed for the neat film. Therefore, the quenching of the early, 1300 nm polymer exciton absorption and blue-shifting correspond to the formation of long-lived polymer polarons from the initial polymer excitons.

We now address in more detail the decay dynamics in the blends. We observe in Figure 6c,d a rapid quenching of the exciton absorption for both blend films. Figure 7 shows the corresponding decays for the F0 and F4 blends at 1330 nm, a wavelength at which the exciton absorption contribution to the signal is dominant. It is apparent that both F0 and F4 exciton absorption signals decay with a time constant τ = 1.8 ± 0.1 ps. This is almost 2 orders of magnitude faster than the corresponding decay dynamics of the neat polymer films.

DOI: 10.1021/acs.chemmater.5b02948
Chem. Mater. 2015, 27, 7934−7944

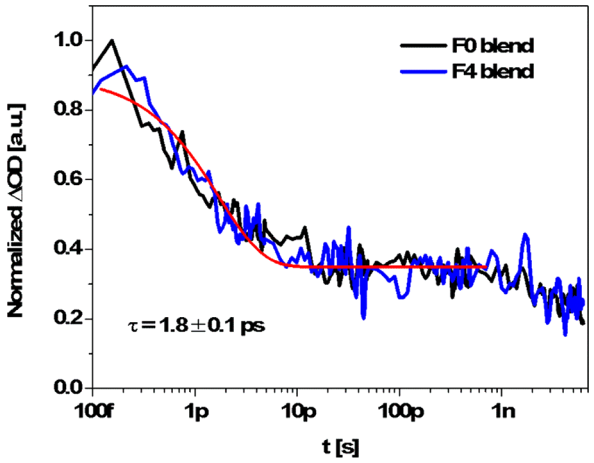

Figure 7. Normalized transient absorption traces of 1:2 F0 and F4 blends with $PC_{70}BM$ excited at 710 nm and 3 $\mu J/cm^2$ and probed at 1330 nm. This decay was assigned to polymer exciton quenching, and therefore (see the text) to charge generation. The red line is a monoexponential fit to the data, with a mean lifetime of 1.8 ± 0.1 ps.

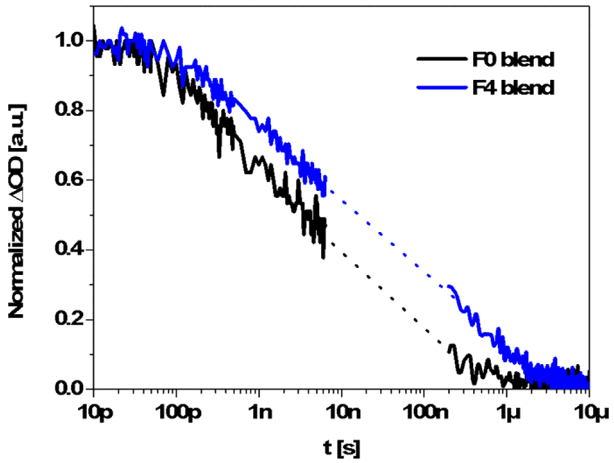

Figure 8. Normalized transient absorption traces of 1:2 F0 and F4 blends with $PC_{70}BM$ excited at 710 nm and 3 $\mu J/cm^2$ probed at 1035 nm. This wavelength was assigned to the polymer polaron (see the text) so that this decay can be associated from ∼50 ps with early charge recombination. The decay is shown at 1035 nm so that the red shift does not contribute to the signal.

This fast quenching of the polymer singlet exciton in the blend films is in agreement with the steady-state PLQ results. For F0 blend films a similar time constant (1.7 ± 0.1 ps; see Figure S8) was observed for the rise of polaron absorption at 788 nm, a wavelength at which there is little interfering absorption from excitons in the neat film (see Figure 6a). We thus conclude that exciton separation to form $F0^+/PC_{70}BM^-$ polaron pairs proceeds in this blend film with a time constant τ = 1.75 ± 0.1 ps. This analysis cannot be carried out for F4 due to the more complex spectral evolution of the neat F4 film spectra; however, we consider 1.8 ps to represent the time constant of the exciton dissociation to form $F4^+/PC_{70}BM^-$ polaron pairs.

Following the rapid (∼1.8 ps) evolution of the photoinduced absorption spectrum from polymer excitons to polarons, the transient polaron absorption in the F0 and F4 blend films exhibits a relatively slow, decay that initiates at ∼50−100 ps and extends to tens of microseconds, as we show in Figure 8. It is apparent from this figure that the polaron decay dynamics, assigned to charge recombination, are approximately 4-fold slower for the F4 blend than the F0 blend, as estimated from the half-lifetime of the polaron decay. These data are monitored at 1035 nm, a wavelength where the red shift of the polaron absorption, discussed below, has minimal impact. The power law nature of these decays and their extension to microsecond time scales, shown in Figure S10, allows them to be assigned to nongeminate recombination. For the F0 blend, similar decay dynamics were observed for the recovery of the GSB (see Figure S9), consistent with the assignment of this decay to nongeminate charge recombination to the ground state.

Note that, for F4, a blue shift of the photoinduced absorption maximum is observed in both the blend and the neat films. As discussed above with respect to the blend films, this blue shift is assigned to polaron formation. The observation of an analogous spectral evolution for the neat F4 film is therefore a strong indicator of a relaxation process of the initially formed F4 excitons into excitons associated with an increased charge transfer or polaron character on the ∼2 ps time scale. The classification of these excitons as intramoleculecular on intermolecular is unclear; however, unless charge transport is highly anisotropic, this has no consequences upon charge separation or collection.

Finally, we observe in Figure 6b,d that the polymer polaron photoinduced bands exhibit a small red shift (from ∼40 ps) of 0.02 eV for the F0 blend (from ∼1170 to 1190 nm) and 0.03 eV for the F4 blend (from 1070 to 1090 nm). A similar red shift of polymer photoinduced absorption has been reported previously for other donor polymers,[22,59] and has been assigned to the energetic relaxation and trapping of the photogenerated polarons.

DISCUSSION

The observations presented herein point out that, upon fluorination, the photophysics of both the neat and the blend polymers are modified. An important result is the similarity in the blue shift of the polymer exciton photoinduced absorbance in the F4 neat and blend films. Since this blue shift was assigned to the polaron pair absorption in the blend film, in the neat film it is associated with the formation of excitons with a partial polaron or charge-transfer character.

The formation of the charge-transfer excitons in the F4 neat film is consistent with our findings of an increased exciton dipole moment upon the insertion of the fluorine atoms via the TD-DFT calculations, which in turn agrees with the idea of a larger exciton delocalization, and thus probably a lower exciton binding energy, resulting in a higher polaron character. The presence of excitations with a high charge-transfer character in neat polymers has been reported before in poly(thienothiophene−benzodithiophene) (PTB)-type polymers in solution[22] as well as in PCDTBT and PCPDTBT oligomers in solution.[34]

We observe that backbone fluorination also has an effect on the exciton dynamics of the neat polymer films. While the decay dynamics of F0 excitons occurs in ∼90 ps, the decay of the charge-transfer excitons in F4 is approximately 2 times slower (∼180 ps). This could indicate that, upon fluorination, species with larger charge character are not only more efficiently formed but are also stabilized within the polymer structure, which is also consistent with the larger $\Delta\mu_{ge}$ calculated in the fluorinated polymer. We note, however, that

DOI: 10.1021/acs.chemmater.5b02948
Chem. Mater. 2015, 27, 7934−7944

the lifetime of these charge-transfer excitons in the F4 neat film (180 ps) is substantially shorter than that of the separated polarons generated in the F4/$PC_{70}BM$ blend (~10 ns), consistent with their assignment to charge-transfer excitons rather than spatially separated polarons.

We turn now to discuss charge generation. Although we do not rule out the contribution of instrument response-limited exciton quenching (charges appearing in less than 100 fs) to the early signal of the blends, the main exciton quenching and polaron formation occurs in ~1.7−1.8 ps for these polymers. This time scale for exciton quenching is consistent with high, but subunity, photoluminescence quenching observed for these blend films.

This picosecond exciton quenching differs from the ultrafast (<100 fs) time scale exciton reported for some other donor−acceptor polymers.[8,59,60] The observation of similar charge generation kinetics in both polymer blends is rather surprising given that the LUMO level of F4 is 0.23 eV lower than that of F0. The ability of F4 to generate charges efficiently despite its lower energy offset may be related to the higher charge-transfer character of F4 polymer excitons. We note that several studies have related a higher degree of charge-transfer character of excitons to improved charge separation properties in both organic and dye-sensitized solar cells.[8,61,62] We also note that the reduced intermixing within the polymer domains in the F4/$PC_{70}BM$ blend may also aid charge separation in this blend.

When comparing the polaron decay dynamics, we observe that nongeminate recombination of F4 blend polarons is at least 4-fold slower as compared to the decay of F0 blend polarons. Slower nongeminate recombination in the F4 blend results in a higher total charge carrier density on the microsecond time scale: with the lowest excitation intensity (0.4 $\mu J/cm^2$), F4 blends present on average a ~60% higher charge density between 200 ns and 1.2 μs, a time scale relevant for charge collection in devices. However, a detailed analysis of charge collection efficiency for these devices is beyond the scope of this study. This finding is similar to the observations in a series of PTB-based polymers, where the signal of the best performing polymer, poly({4,8-bis[(2-ethylhexyl)oxy]benzo-[1,2-*b*:4,5-*b*′]dithiophene-2,6-diyl}{3-fluoro-2-[(2-ethylhexyl)-carbonyl]thieno[3,4-*b*]thiophenediyl}) (PTB7), assigned to the charge-separated state has the slowest recombination time[8] compared to other nonfluorinated and differently structured fluorine-substituted polymers.

We note that the slower nongeminate recombination dynamics observed for F4/$PC_{70}BM$ blends do not appear to result from slower charge carrier mobilities. Field-effect transistor (FET) hole mobilities obtained for these polymers are 3×10^{-3} and 6×10^{-4} cm^2 V s^{-1} for F4 and F0, respectively.[26] This suggests that an additional factor, such as an improved microstructure in the fluorinated F4 polymer blend, favors a spatial separation of holes and electrons and thus slows nongeminate recombination. Indeed, for the F4 blends studied herein, it is likely that the slower nongeminate recombination is a consequence of a microstructure improvement upon fluorination. The F4 blend shows a lower content of fullerene molecules intermixed within the polymer domains, as observed in the polymer PL and inferred from the R-SoXS results. This result is consistent with our observation of an increased polymer aggregation in the F4 blends compared to F0 blends via GIWAXS measurements; the origins of the improved π-stacking in the polymer can be explained by our conformer energetic analysis via DFT calculations. Indeed, the calculations indicate that the planar *s*−*s* conformation is largely preferred by polymer F4, whereas F0 does not exhibit such a preference for either conformation, and as such, it might adopt conformations which would result in a slight twist in the backbone, impeding aggregation and resulting in a higher π-stacking distance. Additionally, the increased $PC_{70}BM$ emission in F4 blends suggests that the more planar, and thus crystallized, polymer backbone also results in the expelling of fullerene molecules, which also contributes to the spatial separation of the free electron and holes and thus results in the slower nongeminate recombination observed. This slower recombination is likely to be responsible, at least in part, for the enhanced device efficiency for the F4 polymer compared to F0.

CONCLUSIONS

In summary, we have found that polymer fluorination can influence not only the polymer energetics but also the change in dipole moment from the ground to the excited state ($\Delta\mu_{ge}$), and the film morphology. The increase in $\Delta\mu_{ge}$ upon fluorination is correlated in the neat fluorinated F4 polymer films with the appearance of an ultrafast (~2 ps) increase in the charge-transfer character of the polymer excitons. The increase in polymer aggregation upon fluorination is correlated with a 4-fold retardation of nongeminate recombination losses. These results thus demonstrate the multiple impacts of polymer fluorination which influence both the material properties and device function, and thus provide further insights into materials design for optimum device performance.

ASSOCIATED CONTENT

Supporting Information

The Supporting Information is available free of charge on the ACS Publications website at DOI: 10.1021/acs.chemmater.5b02948.

UV−vis extinction coefficient, details of $\Delta\mu_{ge}$ calculations and geometries of the dipole moment vectors in the ground and excited states, AFM images, R-SoXS scattering profiles and contrast functions, GIWAXS scattering images and out-of plane and in-plane line-outs, low-intensity TAS traces for F0 and F4 blend films, microsecond-resolved transients in N_2 and O_2 atmospheres in neat and blend films, probed-wavelength dependence in the F4 neat film and fitting parameters, singlet exciton dynamics and polaron dynamics for the F0 blend, and transient absorption kinetics as a function of the beam intensity on the microsecond scale (PDF)

AUTHOR INFORMATION

Corresponding Authors

*E-mail: z.fei@imperial.ac.uk.
*E-mail: j.durrant@imperial.ac.uk.
*E-mail: m.heeney@imperial.ac.uk.

Notes

The authors declare no competing financial interest.

ACKNOWLEDGMENTS

We gratefully acknowledge the Engineering and Physical Sciences Research Council (EPSRC) (Grants EP/1019278/1 and EP/K011987/1) for funding. E.C.-F. also thanks the Consejo Nacional de Ciencia y Tecnología (CONACyT) (Scholarship 309929) and the Kernahan Fund, Imperial College London, for funding. C.R.M. thanks the Australian

DOI: 10.1021/acs.chemmater.5b02948
Chem. Mater. 2015, 27, 7934−7944

Research Council for funding (Grant FT100100275). C.R.M. and E.G. acknowledge travel funding provided by the International Synchrotron Access Program (ISAP) managed by the Australian Synchrotron and funded by the Australian Government. Part of this work was performed at the SAXS/WAXS beamline at the Australian Synchrotron, Victoria, Australia, and at beamline 11.0.1.2 of the Advanced Light Source at Lawrence Berkeley National Laboratory.

REFERENCES

(1) Kroon, R.; Lenes, M.; Hummelen, J. C.; Blom, P. W. M.; de Boer, B. Small Bandgap Polymers for Organic Solar Cells (Polymer Material Development in the Last 5 Years). *Polym. Rev.* **2008**, *48*, 531−582.

(2) Etxebarria, I.; Ajuria, J.; Pacios, R. Polymer:fullerene Solar Cells: Materials, Processing Issues, and Cell Layouts to Reach Power Conversion Efficiency over 10%, a Review. *J. Photonics Energy* **2015**, *5*, 057214.

(3) Liu, C.; Yi, C.; Wang, K.; Yang, Y.; Bhatta, R. S.; Tsige, M.; Xiao, S.; Gong, X. Single-Junction Polymer Solar Cells with Over 10% Efficiency by a Novel Two-Dimensional Donor−Acceptor Conjugated Copolymer. *ACS Appl. Mater. Interfaces* **2015**, *7*, 4928−4935.

(4) Ye, L.; Zhang, S.; Zhao, W.; Yao, H.; Hou, J. Highly Efficient 2D-Conjugated Benzodithiophene-Based Photovoltaic Polymer with Linear Alkylthio Side Chain. *Chem. Mater.* **2014**, *26*, 3603−3605.

(5) Meyer, F. Fluorinated Conjugated Polymers in Organic Bulk Heterojunction Photovoltaic Solar Cells. *Prog. Polym. Sci.* **2015**, *47*, 70−91.

(6) Liu, Y.; Zhao, J.; Li, Z.; Mu, C.; Ma, W.; Hu, H.; Jiang, K.; Lin, H.; Ade, H.; Yan, H. Aggregation and Morphology Control Enables Multiple Cases of High-Efficiency Polymer Solar Cells. *Nat. Commun.* **2014**, *5*, 5293.

(7) Son, H. J.; Wang, W.; Xu, T.; Liang, Y.; Wu, Y.; Li, G.; Yu, L. Synthesis of Fluorinated Polythienothiophene-Co-Benzodithiophenes and Effect of Fluorination on the Photovoltaic Properties. *J. Am. Chem. Soc.* **2011**, *133*, 1885−1894.

(8) Carsten, B.; Szarko, J. M.; Son, H. J.; Wang, W.; Lu, L.; He, F.; Rolczynski, B. S.; Lou, S. J.; Chen, L. X.; Yu, L. Examining the Effect of the Dipole Moment on Charge Separation in Donor-Acceptor Polymers for Organic Photovoltaic Applications. *J. Am. Chem. Soc.* **2011**, *133*, 20468−20475.

(9) Price, S. C.; Stuart, a. C.; Yang, L. G.; Zhou, H. X.; You, W. Fluorine Substituted Conjugated Polymer of Medium Bandwidth Yield 7% Efficiency in Polymer-Fullerine Solar Cells. *J. Am. Chem. Soc.* **2011**, *133*, 4625−4631.

(10) Iyer, A.; Bjorgaard, J.; Anderson, T.; Kose, M. E. Quinoxaline-Based Semiconducting Polymers: Effect of Fluorination on the Photophysical, Thermal and Charge Transport Properties. *Macromolecules* **2012**, *45*, 6380−6389.

(11) Schroeder, B. C.; Huang, Z.; Ashraf, R. S.; Smith, J.; D'Angelo, P.; Watkins, S. E.; Anthopoulos, T. D.; Durrant, J. R.; McCulloch, I. Silaindacenodithiophene-Based Low Band Gap Polymers - The Effect of Fluorine Substitution on Device Performances and Film Morphologies. *Adv. Funct. Mater.* **2012**, *22*, 1663−1670.

(12) Albrecht, S.; Janietz, S.; Schindler, W.; Frisch, J.; Kurpiers, J.; Kniepert, J.; Inal, S.; Pingel, P.; Fostiropoulos, K.; Koch, N.; Neher, D. Fluorinated Copolymer PCPDTBT with Enhanced Open-Circuit Voltage and Reduced Recombination for Highly Efficient Polymer Solar Cells. *J. Am. Chem. Soc.* **2012**, *134*, 14932−14944.

(13) Stuart, A. C.; Tumbleston, J. R.; Zhou, H.; Li, W.; Liu, S.; Ade, H.; You, W. Fluorine Substituents Reduce Charge Recombination and Drive Structure and Morphology Development in Polymer Solar Cells. *J. Am. Chem. Soc.* **2013**, *135*, 1806−1815.

(14) Yang, L.; Tumbleston, J.; Zhou, H.; Ade, H.; You, W. Disentangling the Impact of Side Chains and Fluorine Substituents of Conjugated Donor Polymers on the Performance of Photovoltaic Blends. *Energy Environ. Sci.* **2013**, *6*, 316−326.

(15) Li, W.; Albrecht, S.; Yang, L.; Roland, S.; Tumbleston, J. R.; McAfee, T.; Yan, L.; Kelly, M. A.; Ade, H.; Neher, D.; You, W. Mobility-Controlled Performance of Thick Solar Cells Based on Fluorinated Copolymers. *J. Am. Chem. Soc.* **2014**, *136*, 15566.

(16) Tumbleston, J. R.; Collins, B. a.; Yang, L.; Stuart, A. C.; Gann, E.; Ma, W.; You, W.; Ade, H. The Influence of Molecular Orientation on Organic Bulk Heterojunction Solar Cells. *Nat. Photonics* **2014**, *8*, 385−391.

(17) He, X.; Mukherjee, S.; Watkins, S.; Chen, M.; Qin, T.; Thomsen, L.; Ade, H.; McNeill, C. R. On the Influence of Fluorination and Molecular Weight on the Morphology and Performance of PTB7: PC71BM Solar Cells. *J. Phys. Chem. C* **2014**, *118*, 9918−9929.

(18) Bronstein, H.; Frost, J. M.; Hadipour, A.; Kim, Y.; Nielsen, C. B.; Ashraf, R. S.; Rand, B. P.; Watkins, S.; McCulloch, I. Effect of Fluorination on the Properties of a Donor − Acceptor Copolymer for Use in Photovoltaic Cells and Transistors. *Chem. Mater.* **2013**, *25*, 277−285.

(19) Wang, H.; Yu, X.; Yi, C.; Ren, H.; Liu, C.; Yang, Y.; Xiao, S.; Zheng, J.; Karim, A.; Cheng, S. Z. D.; Gong, X. Fine-Tuning of Fluorinated thieno[3,4-B]thiophene Copolymer for Efficient Polymer Solar Cells. *J. Phys. Chem. C* **2013**, *117*, 4358−4363.

(20) Dimitrov, S. D.; Huang, Z.; Deledalle, F.; Nielsen, C. B.; Schroeder, B. C.; Ashraf, R. S.; Shoaee, S.; McCulloch, I.; Durrant, J. R. Towards Optimisation of Photocurrent from Fullerene Excitons in Organic Solar Cells. *Energy Environ. Sci.* **2014**, *7*, 1037.

(21) Carsten, B.; Szarko, J. M.; Lu, L.; Son, H. J.; He, F.; Botros, Y. Y.; Chen, L. X.; Yu, L. Mediating Solar Cell Performance by Controlling the Internal Dipole Change in Organic Photovoltaic Polymers. *Macromolecules* **2012**, *45*, 6390−6395.

(22) Rolczynski, B. S.; Szarko, J. M.; Son, H. J.; Liang, Y.; Yu, L.; Chen, L. X. Ultrafast Intramolecular Exciton Splitting Dynamics in Isolated Low-Band-Gap Polymers and Their Implications in Photovoltaic Materials Design. *J. Am. Chem. Soc.* **2012**, *134*, 4142−4152.

(23) Homyak, P. D.; Tinkham, J.; Lahti, P. M.; Coughlin, E. B. Thieno [3,4-B] Thiophene Acceptors with Alkyl, Aryl, Perfluoroalkyl, and Perfluorophenyl Pendants for Donor − Acceptor Low Bandgap Polymers. *Macromolecules* **2013**, *46*, 8873−8881.

(24) Homyak, P.; Liu, Y.; Ferdous, S.; Liu, F.; Russell, T. P.; Coughlin, E. B. Effect of Pendant Functionality in Thieno[3,4- B]thiophene- Alt -Benzodithiophene Polymers for OPVs. *Chem. Mater.* **2015**, *27*, 443−449.

(25) Xu, T.; Lu, L.; Zheng, T.; Szarko, J. M.; Schneider, A.; Chen, L. X.; Yu, L. Tuning the Polarizability in Donor Polymers with a Thiophenesaccharin Unit for Organic Photovoltaic Applications. *Adv. Funct. Mater.* **2014**, *24*, 3432.

(26) Fei, Z.; Shahid, M.; Yaacobi-Gross, N.; Rossbauer, S.; Zhong, H.; Watkins, S. E.; Anthopoulos, T. D.; Heeney, M. Thiophene Fluorination to Enhance Photovoltaic Performance in Low Band Gap Donor − Acceptor Polymers. *Chem. Commun.* **2012**, *48*, 11130−11132.

(27) Frisch, M. J.; Trucks, G. W.; Schlegel, H. B.; Scuseria, G. E.; Robb, M. A.; Cheeseman, J. R.; Scalmani, G.; Barone, V.; Mennucci, B.; Petersson, G. A.; Nakatsuji, H.; Caricato, M.; Li, X.; Hratchian, H. P.; Izmaylov, A. F.; Bloino, J.; Zheng, G.; Sonnenberg, J. L.; Hada, M.; Ehara, M.; Toyota, K.; Fukuda, R.; Hasegawa, J.; Ishida, M.; Nakajima, T.; Honda, Y.; Kitao, O.; Nakai, H.; Vreven, T.; Montgomery, Jr., J. A.; Peralta, J. E.; Ogliaro, F.; Bearpark, M.; Heyd, J. J.; Brothers, E.; Kudin, K. N.; Staroverov, V. N.; Kobayashi, R.; Normand, J.; Raghavachari, K.; Rendell, A.; Burant, J. C.; Iyengar, S. S.; Tomasi, J.; Cossi, M.; Rega, N.; Millam, J. M.; Klene, M.; Knox, J. E.; Cross, J. B.; Bakken, V.; Adamo, C.; Jaramillo, J.; Gomperts, R.; Stratmann, R. E.; Yazyev, O.; Austin, A. J.; Cammi, R.; Pomelli, C.; Ochterski, J. W.; Martin, R. L.; Morokuma, K.; Zakrzewski, V. G.; Voth, G. A.; Salvador, P.; Dannenberg, J. J.; Dapprich, S.; Daniels, A. D.; Farkas, Ö.; Foresman, J. B.; Ortiz, J. V.; Cioslowski, J.; Fox, D. J. *Gaussian 09*, revision C.01; Gaussian, Inc.: Wallingford, CT, 2009.

(28) Jamieson, F. C.; Domingo, E. B.; McCarthy-Ward, T.; Heeney, M.; Stingelin, N.; Durrant, J. R. Fullerene Crystallisation as a Key Driver of Charge Separation in Polymer/fullerene Bulk Heterojunction Solar Cells. *Chem. Sci.* **2012**, *3*, 485.

DOI: 10.1021/acs.chemmater.5b02948
Chem. Mater. 2015, 27, 7934−7944

(29) Mikhnenko, O. V.; Azimi, H.; Scharber, M.; Morana, M.; Blom, P. W. M.; Loi, M. A. Exciton Diffusion Length in Narrow Bandgap Polymers. *Energy Environ. Sci.* **2012**, *5*, 6960−6965.
(30) Bruno, A.; Reynolds, L. X.; Dyer-Smith, C.; Nelson, J.; Haque, S. A. Determining the Exciton Diffusion Length in a Polyfluorene from Ultrafast Fluorescence Measurements of Polymer/Fullerene Blend Films. *J. Phys. Chem. C* **2013**, *117*, 19832−19838.
(31) Cook, S.; Furube, A.; Katoh, R.; Han, L. Estimate of Singlet Diffusion Lengths in PCBM Films by Time-Resolved Emission Studies. *Chem. Phys. Lett.* **2009**, *478*, 33−36.
(32) Kirby, N. M.; Mudie, S. T.; Hawley, A. M.; Cookson, D. J.; Mertens, H. D. T.; Cowieson, N.; Samardzic-Boban, V. A Low-Background-Intensity Focusing Small-Angle X-Ray Scattering Undulator Beamline. *J. Appl. Crystallogr.* **2013**, *46*, 1670−1680.
(33) Gann, E.; Young, a. T.; Collins, B. a.; Yan, H.; Nasiatka, J.; Padmore, H. a.; Ade, H.; Hexemer, A.; Wang, C. Soft X-Ray Scattering Facility at the Advanced Light Source with Real-Time Data Processing and Analysis. *Rev. Sci. Instrum.* **2012**, *83*, 045110.
(34) Scarongella, M.; Laktionov, A.; Rothlisberger, U.; Banerji, N. Charge Transfer Relaxation in Donor−acceptor Type Conjugated Materials. *J. Mater. Chem. C* **2013**, *1*, 2308.
(35) Chai, J.-D.; Head-Gordon, M. Long-Range Corrected Hybrid Density Functionals with Damped Atom-Atom Dispersion Corrections. *Phys. Chem. Chem. Phys.* **2008**, *10*, 6615−6620.
(36) Sutton, C.; Körzdörfer, T.; Gray, M. T.; Brunsfeld, M.; Parrish, R. M.; Sherrill, C. D.; Sears, J. S.; Brédas, J. L. Accurate Description of Torsion Potentials in Conjugated Polymers Using Density Functionals with Reduced Self-Interaction Error. *J. Chem. Phys.* **2014**, *140*, 054310.
(37) Jackson, N. E.; Savoie, B. M.; Kohlstedt, K. L.; Olvera de la Cruz, M.; Schatz, G. C.; Chen, L. X.; Ratner, M. A. Controlling Conformations of Conjugated Polymers and Small Molecules: The Role of Nonbonding Interactions. *J. Am. Chem. Soc.* **2013**, *135*, 10475−10483.
(38) Osaka, I.; Shimawaki, M.; Mori, H.; Doi, I.; Miyazaki, E.; Koganezawa, T.; Takimiya, K. Synthesis, Characterization, and Transistor and Solar Cell Applications of a Naphthobisthiadiazole-Based Semiconducting Polymer. *J. Am. Chem. Soc.* **2012**, *134*, 5425.
(39) Son, H. J.; Wang, W.; Xu, T.; Liang, Y.; Wu, Y.; Li, G.; Yu, L. Synthesis of Fluorinated Polythienothiophene-Co-Benzodithiophenes and Effect of Fluorination on the Photovoltaic Properties. *J. Am. Chem. Soc.* **2011**, *133*, 1885−1894.
(40) Nielsen, C. B.; White, A. J. P.; McCulloch, I. Effect of Fluorination of 2,1,3-Benzothiadiazole. *J. Org. Chem.* **2015**, *80*, 5045−5048.
(41) Bronstein, H.; Frost, J. M.; Hadipour, A.; Kim, Y.; Nielsen, C. B.; Ashraf, R. S.; Rand, B. P.; Watkins, S.; McCulloch, I. Effect of Fluorination on the Properties of a Donor−Acceptor Copolymer for Use in Photovoltaic Cells and Transistors. *Chem. Mater.* **2013**, *25*, 277−285.
(42) Fei, Z.; Boufflet, P.; Wood, S.; Wade, J.; Moriarty, J.; Gann, E.; Ratcliff, E. L.; McNeill, C. R.; Sirringhaus, H.; Kim, J.-S.; Heeney, M. Influence of Backbone Fluorination in Regioregular Poly(3-Alkyl-4-Fluoro)thiophenes. *J. Am. Chem. Soc.* **2015**, *137*, 6866−6879.
(43) Kohn, P.; Rong, Z.; Scherer, K. H.; Sepe, A.; Sommer, M.; Müller-Buschbaum, P.; Friend, R. H.; Steiner, U.; Hüttner, S. Crystallization-Induced 10-Nm Structure Formation in P3HT/PCBM Blends. *Macromolecules* **2013**, *46*, 4002−4013.
(44) Jo, J. W.; Jung, J. W.; Wang, H. W.; Kim, P.; Russell, T. P.; Jo, W. H. Fluorination of Polythiophene Derivatives for High Performance Organic Photovoltaics. *Chem. Mater.* **2014**, *26*, 4214−4220.
(45) Collins, B. a.; Li, Z.; Tumbleston, J. R.; Gann, E.; McNeill, C. R.; Ade, H. Absolute Measurement of Domain Composition and Nanoscale Size Distribution Explains Performance in PTB7:PC71bm Solar Cells. *Adv. Energy Mater.* **2013**, *3*, 65−74.
(46) Nguyen, T. L.; Choi, H.; Ko, S.-J.; Uddin, M. a.; Walker, B.; Yum, S.; Jeong, J.-E.; Yun, M. H.; Shin, T. J.; Hwang, S.; Kim, J. Y.; Woo, H. Y. Semi-Crystalline Photovoltaic Polymers with Efficiency Exceeding 9% in a ∼ 300 Nm Thick Conventional Single-Cell Device. *Energy Environ. Sci.* **2014**, *7*, 3040−3051.
(47) Yamamoto, S.; Ohkita, H.; Benten, H.; Ito, S. Role of Interfacial Charge Transfer State in Charge Generation and Recombination in Low-Bandgap Polymer Solar Cell. *J. Phys. Chem. C* **2012**, *116*, 14804−14810.
(48) Albert-Seifried, S.; Ko, D.-H.; Hüttner, S.; Kanimozhi, C.; Patil, S.; Friend, R. H. Efficiency Limitations in a Low Band-Gap Diketopyrrolopyrrole-Based Polymer Solar Cell. *Phys. Chem. Chem. Phys.* **2014**, *16*, 6743−6752.
(49) Dimitrov, S. D.; Wheeler, S.; Niedzialek, D.; Schroeder, B. C.; Utzat, H.; Frost, J. M.; Yao, J.; Gillett, A.; Tuladhar, P. S.; McCulloch, I.; Nelson, J.; Durrant, J. R. Polaron Pair Mediated Triplet Generation in Polymer/fullerene Blends. *Nat. Commun.* **2015**, *6*, 6501.
(50) Amao, Y.; Asai, K.; Okura, I. High Sensitive Oxygen Sensor Based on Quenching of Triplet-Triplet Absorption of Fullerene C60-Polystyrene Film. *Bull. Chem. Soc. Jpn.* **1999**, *72*, 2223.
(51) Foley, S.; Bosi, S.; Larroque, C.; Prato, M.; Janot, J.; Seta, P. Photophysical Properties of Novel Water Soluble Fullerene Derivatives. *Chem. Phys. Lett.* **2001**, *350*, 198−205.
(52) Ohkita, H.; Cook, S.; Astuti, Y.; Duffy, W.; Tierney, S.; Zhang, W.; Heeney, M.; McCulloch, I.; Nelson, J.; Bradley, D. D. C.; Durrant, J. R. Charge Carrier Formation in Polythiophene/fullerene Blend Films Studied by Transient Absorption Spectroscopy. *J. Am. Chem. Soc.* **2008**, *130*, 3030−3042.
(53) Soon, Y. W.; Shoaee, S.; Ashraf, R. S.; Bronstein, H.; Schroeder, B. C.; Zhang, W.; Fei, Z.; Heeney, M.; McCulloch, I.; Durrant, J. R. Material Crystallinity as a Determinant of Triplet Dynamics and Oxygen Quenching in Donor Polymers for Organic Photovoltaic Devices. *Adv. Funct. Mater.* **2014**, *24*, 1474−1482.
(54) Nelson, J. Diffusion-Limited Recombination in Polymer-Fullerene Blends and Its Influence on Photocurrent Collection. *Phys. Rev. B: Condens. Matter Mater. Phys.* **2003**, *67*, 155209.
(55) Nogueira, A. F.; Montanari, I.; Nelson, J.; Durrant, J. R.; Winder, C.; Sariciftci, N. S.; Brabec, C. Charge Recombination in Conjugated Polymer/Fullerene Blended Films Studied by Transient Absorption Spectroscopy. *J. Phys. Chem. B* **2003**, *107*, 1567−1573.
(56) Clarke, T. M.; Jamieson, F. C.; Durrant, J. R. Transient Absorption Studies of Bimolecular Recombination Dynamics in Polythiophene/Fullerene Blend Films. *J. Phys. Chem. C* **2009**, *113*, 20934−20941.
(57) Clarke, T. M.; Ballantyne, A. M.; Tierney, S.; Heeney, M.; Duffy, W.; McCulloch, I.; Nelson, J.; Durrant, J. R. Charge Photogeneration in Low Band Gap Polyselenophene/Fullerene Blend Films. *J. Phys. Chem. C* **2010**, *114*, 8068−8075.
(58) Shoaee, S.; Subramaniyan, S.; Xin, H.; Keiderling, C.; Tuladhar, P. S.; Jamieson, F.; Jenekhe, S. a.; Durrant, J. R. Charge Photogeneration for a Series of Thiazolo-Thiazole Donor Polymers Blended with the Fullerene Electron Acceptors PCBM and ICBA. *Adv. Funct. Mater.* **2013**, *23*, 3286−3298.
(59) Etzold, F.; Howard, I. a; Mauer, R.; Meister, M.; Kim, T.-D.; Lee, K.-S.; Baek, N. S.; Laquai, F. Ultrafast Exciton Dissociation Followed by Nongeminate Charge Recombination in PCDTBT:PCBM Photovoltaic Blends. *J. Am. Chem. Soc.* **2011**, *133*, 9469−9479.
(60) Grancini, G.; Maiuri, M.; Fazzi, D.; Petrozza, a; Egelhaaf, H.-J.; Brida, D.; Cerullo, G.; Lanzani, G. Hot Exciton Dissociation in Polymer Solar Cells. *Nat. Mater.* **2012**, *12*, 29−33.
(61) Hwang, I.; Beaupré, S.; Leclerc, M.; Scholes, G. D. Ultrafast Relaxation of Charge-Transfer Excitons in Low-Bandgap Conjugated Copolymers. *Chem. Sci.* **2012**, *3*, 2270.
(62) Listorti, A.; O'Regan, B.; Durrant, J. R. Electron Transfer Dynamics in Dye-Sensitized Solar Cells. *Chem. Mater.* **2011**, *23*, 3381−3399.

DOI: 10.1021/acs.chemmater.5b02948
Chem. Mater. 2015, 27, 7934−7944